Int. J. Heat Mass Transfer. Vol. 33, No. 6, pp. 1307–1319, 1990
Printed in Great Britain

0017–9310/90 $3.00 + 0.00

Experimental measurements of orthogonal mixed convection in a partial enclosure

M. M. RAHMAN
Mechanical and Materials Engineering Department, Wright State University, Dayton, OH 45435, U.S.A.

and

V. P. CAREY
Department of Mechanical Engineering, University of California, Berkeley, CA 94720, U.S.A.

(*Received* 17 *May* 1989 *and in final form* 6 *September* 1989)

Abstract—Measurements of local heat transfer coefficients and results of flow visualization experiments are presented for orthogonal mixed convection in a partial enclosure with uniformly heated side walls and adiabatic top and bottom walls. In this study, experiments using water as a test fluid are conducted in a small scale test section with different inlet and outlet configurations. The flow and heating conditions are chosen to simulate the high Rayleigh number (10^{10}–10^{11}) and low to moderate Reynolds number (0–9000) typically encountered in building heat transfer applications. As the flow rate through the enclosure increases, the enhancement of heat transfer above that for natural convection alone also increases. The local enhancement is as large as a factor of 7 for some flow situations. The variation of local heat transfer coefficient over the heated surface is found to be strongly affected by the recirculation of portions of the forced flow within the enclosure as well as the impingement on or separation of flow from the side walls in some regions. Mean heat transfer coefficients for the side walls are also reported here, which are determined by averaging the measured local values over the heated surface. The highest average enhancement is a factor of 2.6 at $Ra = 1.6 \times 10^{10}$ and $Re = 8740$ for a staggered orientation of the inlet and exit apertures. Correlations for the mean heat transfer coefficient and a flow regime map for different enclosure geometries are also proposed.

INTRODUCTION

CROSS-FLOW mixed convection in partial enclosure geometries may arise in several thermal control applications. Flow in a room, for example, is often driven by a combination of horizontal forced flow due to ventilation and a buoyancy driven flow along the walls resulting from the difference between the wall temperature and the bulk air temperature. Similar flows may arise in the cooling system of a computer or any other electronic equipment when a horizontal flow of air through a cabinet containing heat dissipating electronic components on vertical circuit boards.

This type of enclosure flow is somewhat related to the mixed convection in a horizontal tube or duct, particularly near the entrance when the flow rate is small. Experimental studies of mixed convection in a tube with uniformly heated surface condition have been reported by, among others, McComas and Eckert [1], Mori *et al.* [2], Petukov and Polyakov [3], Shanon and Depew [4], Bergles and Simonds [5], Hong *et al.* [6] and Morcos and Bergles [7]. These studies used either air, water or ethylene glycol as the test fluid and obtained heat transfer data covering wide ranges of Reynolds and Grashof numbers. Correlations for the heat transfer coefficient were also developed based on the experimental data. Variable fluid property and wall conduction effects were also investigated. The transition of the flow from laminar to turbulent was found to be somewhat dependent on the wall heat flux. The experimental studies for tubes with an isothermal surface condition have recently been summarized by Yousef and Tarasuk [8]. For both isothermal and uniformly heated surface conditions, it was apparent that the experimental data cannot be correlated by using a simple superposition of forced and free convection effects (i.e. simple summation of the h values for each mechanism).

Several analytical and numerical studies of mixed convection in horizontal tubes have also been performed. The ones more related to the present study are those dealing with the hydrodynamic and/or thermally developing flow. Ou and Cheng [9] and Cheng and Ou [10] employed a numerical finite difference scheme to determine natural convection effects on laminar flow near the entrance of a horizontal tube. Based on the high Prandtl number approximation, they assumed that the axial flow field in the entrance region retained the Poiseuille flow profile and that the secondary flow is important only in the energy equation. Their results agreed reasonably well with experimental measurements for high Prandtl number fluids. Recently, Hishida *et al.* [11] solved this type of entrance flow problem without using the large

NOMENCLATURE

a	exponent for equation (5)
b	exponent for equation (5)
d	hydraulic diameter for test section
g	gravitational acceleration
Gr^*	Grashof number based on heat flux, $g\beta qL^4/kv^2$
h	local heat transfer coefficient
$\bar{h}$	mean heat transfer coefficient
k	fluid thermal conductivity
L	length of the test section
n	exponent for equation (4)
Pr	Prandtl number
q	surface heat flux
Ra^*	Rayleigh number based on surface heat flux, $Gr^* Pr$
Re	Reynolds number
x	vertical coordinate
z	horizontal coordinate parallel to heated surface.

Greek symbols

β	coefficient of volumetric expansion
Γ	ratio of average forced to natural convection ($\bar{h}_{fc}/\bar{h}_{nc}$)
ν	fluid kinematic viscosity.

Subscripts

d	based on hydraulic diameter
fc	forced convection
m	based on maximum length
mc	mixed convection
nc	natural convection
x	based on x
z	based on z.

Prandtl number approximation. They also extended it to circumstances where both hydrodynamic and thermal boundary layers were developing. Computations were done for a wide range of flow and heating conditions. An analytical solution for the hydrodynamically and thermally developing flow in an isothermally heated tube was reported by Yao [12]. He used an asymptotic expansion technique by perturbing the developing flow in an unheated pipe.

Mixed convection during developing flow in a horizontal rectangular channel has also been investigated by Ou *et al.* [13] for an isothermal wall condition and by Cheng *et al.* [14] and Abou-Ellail and Morcos [15] for uniformly heated surface conditions. These numerical studies calculated the flow field and the heat transfer coefficient for Prandtl numbers ranging from 1 to 20. It was found that an increase in Rayleigh number results in a reduction of the entry length and an enhancement of the heat transfer coefficient. These developing flow studies in a rectangular channel are more directly related to enclosure flows because of their boundary layer structure near the wall. However, in most enclosure configurations, such as the inside of a room in a building or in a cabinet housing electronic circuit boards, all of the sides are not kept at an identical condition. Often the ceiling and the floor may have quite different temperature or heat flux conditions than those of the side walls. Moreover, the studies mentioned above considered flows at Rayleigh numbers of 10^5 or lower, which is much smaller than a typical Rayleigh number for building heat transfer circumstances. Therefore, the results of the pipe or duct flows described above cannot be directly applied to flows of this type.

In two recent studies, Johnson *et al.* [16] and Neiswanger *et al.* [17] presented experimental data for flows in rectangular enclosures with high Rayleigh and low to moderate Reynolds numbers that are typical of building heat transfer circumstances. The data reported by Johnson *et al.* [16] deal with a rectangular channel with uniformly heated side walls and adiabatic top and bottom walls. The ends of the channels were open to fluid reservoirs. The flow inside the enclosure was found to be somewhat similar to the flow in a rectangular duct, except for the presence of strong vertical natural convection effects near the heated walls. The experimental conditions ranged from pure natural convection to strong forced convection where buoyancy effects were negligible. The experimental data presented in Neiswanger *et al.* [17] were taken with flow and heat transfer conditions similar to those of Johnson *et al.* [16], except for the fact that the entrance and the exit to the test section were restricted with identical doorways. The flow and heat transfer inside the enclosure were found to be quite significantly affected by the presence of these restrictions. Depending on the flow rate, one or more recirculation regions were found to be present inside the enclosure.

Even though the studies by Johnson *et al.* [16] and Neiswanger *et al.* [17] revealed a number of interesting features of cross-flow mixed convection in a rectangular enclosure, results were obtained for only two specific flow situations, namely an open-ended rectangular enclosure and an enclosure with identical doorways at the inlet and the exit. Moreover, the trend of the distribution of the local heat transfer coefficient in these two cases confirmed that restrictions on the path of the flow have a very strong influence on the flow and heat transfer behavior.

The studies discussed above indicate that some specific areas of orthogonal mixed convection have been quite well explored. However, many questions are as yet unanswered for the high Rayleigh number

flows which may arise in buildings and cooling systems for electronic equipment. The present experimental efforts were undertaken to obtain more information about such flows. Experiments were conducted for internal flow in a rectangular partial enclosure with three different inlet and outlet opening configurations. They were (a) a door at the entrance with open-ended exit, (b) a door at the exit with open-ended entrance, and (c) non-symmetric restrictions at the inlet and the exit. The test section used in these experiments had uniformly heated vertical side walls, adiabatic top and bottom walls and openings at the other two walls which were also adiabatic in nature. The structures of the flows were observed visually using a dye injection technique. The values of the local heat transfer coefficient at different locations on the plate were measured. These were integrated to calculate the mean heat transfer coefficient for different flow and heat flux conditions. Correlating equations for the mean heat transfer coefficient and the flow regime transition maps were also developed for different enclosure configurations.

EXPERIMENTAL APPARATUS AND PROCEDURE

The test section used for the experiments reported here is shown in Fig. 1. Within the enclosure, the cross-section normal to the forced flow direction is a square 20.0 cm high and 20.0 cm wide, and the top and bottom walls of the test section are made of 12.7 mm thick transparent acrylic plastic. This allowed the flow to be observed when employing the flow visualization techniques. For the tests with water reported here, the heat transfer through the plastic was negligible, so the top and bottom walls were essentially adiabatic. The end walls (doorways) were also made of acrylic plastic and were also adiabatic during the experiments.

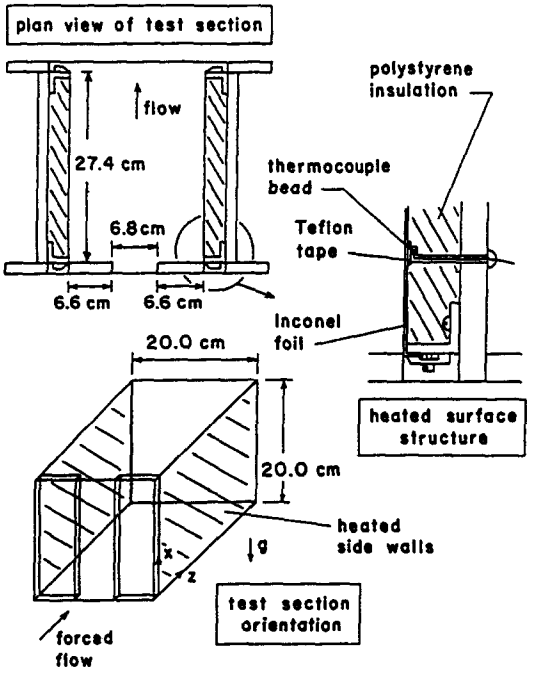

FIG. 1. Test section for mixed convection experiments.

In the test section, along each vertical side wall, two jaw assemblies were used to stretch a 0.0264 mm thick sheet of Inconel foil over a 25.4 mm thick layer of polystyrene foam insulation. The foil was also bonded to the surface of the insulation, except at the thermocouple locations. The foil was very uniform in thickness (± 0.0013 mm) so that when an electric current passed through it, a uniform heat flux condition was imposed along the vertical walls of the enclosure. The polystyrene insulation virtually eliminated heat loss to the surroundings, so all the applied heat was delivered to the water. In addition, due to the thinness of the Inconel foil, conduction of heat in the wall structure was negligible.

An array of copper–constantan thermocouples was used to determine the local wall temperature. These thermocouples were installed behind the foil as shown in Fig. 1. A thin layer of teflon tape was used between each thermocouple bead and the foil to prevent any electrical interference which might have affected the thermocouple reading, while maintaining good thermal communication between the bead and the foil. Thermocouple wires leaving the test section were sealed using RTV silicone to prevent any water leakage. One side wall was instrumented with 32 thermocouples distributed over the surface of the wall. The opposite side wall had only six thermocouples to verify the symmetry of thermal transport from the two walls during the tests with symmetric doorways. Two thermocouples mounted on a support rod at different elevations at the entrance of the test section were used to determine the ambient (and core flow) water temperature.

The flow of water through the test section was supplied by the flow system shown schematically in Fig. 2. Water from the storage reservoir flowed into the test section and was discharged into the exit plenum. The water then passed through the pump and flow meter and was returned to the inlet reservoir through an overhead pipe.

The inlet reservoir is a large tank with a capacity of 246 liters. The water return line splits into two parts just before entering the reservoir to reduce the kinetic energy of the return flow. Below the water level in the tank, each return line has a staggered hole pattern around its circumference and a capped end. This distributes water as evenly as possible for a greater flow uniformity in the tank. One layer of nylon window-screen material was located about halfway between the water return line and the test section inlet to help damp out any flow irregularities. The flow visualization studies indicated that the inlet flow was, in fact, laminar and very symmetrical with respect to the rectangular inlet cross-section.

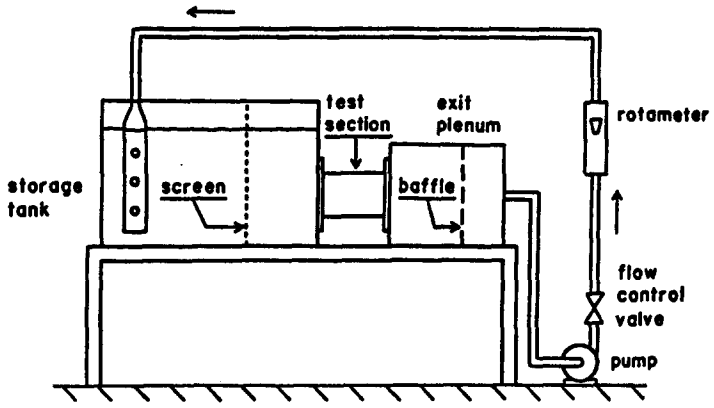

FIG. 2. Schematic of the flow loop for mixed convection experiments.

The exit plenum is slightly larger than the test section, having a capacity of 76 liters. An acrylic plastic distribution plate with a staggered array of small holes was installed inside the exit plenum to prevent premature flow constriction in the test section. The plumbing lines in the water circulation loop were 31.8 mm i.d. PVC pipe. To help isolate the test section from the pump vibration, flexible rubber couplers were used to connect the pump inlet and outlet to the hard piping in the system. A calibrated rotameter manufactured by King Instruments, with a range of 23–110 l min^{-1}, was used to determine the water flow rate. A centrifugal pump from Price Pump Company was used to pump water through the system. A gate valve between the pump and the rotameter was used to control the flow rate.

The electric power required to heat the walls of the test section was provided by a Sorensen DCR 40-40B 1800 W regulated d.c. power supply. A specified current of up to 45 A was passed through the Inconel foil, establishing a uniform heat flux at the walls to a limit of 1900 W m^{-2}. The current through the foil was determined by measuring the voltage drop across a large shunt resistor of known resistance in the circuit. This measurement was taken using a Hewlett–Packard 3446A digital multimeter. The copper–constantan thermocouples in the test section were read using an Omega two-pole sector switch and a precision Fluke digital readout.

The experimental system permitted testing over Rayleigh numbers (Ra^*_{xm}) and inside channel Reynolds numbers (Re_d) in the ranges $5 \times 10^9 < Ra^*_{xm} < 10^{11}$ and $670 < Re_d < 7000$. The lower limits of these ranges were determined by the minimum flow and heat flux conditions for which accurate measurements were possible. The upper limits corresponded to the output capacity of the equipment.

Experiments were performed for three different entrance and exit configurations in the test section. These are sketched in Fig. 3. In each case, the aperture extended from the bottom to the top of the test section. In the inlet and exit aperture configurations, the opening was 6.8 cm wide at the restricted side, and fully open on the other side. In the staggered aperture configuration, the openings were 13.4 cm wide, or about two-thirds of the enclosure width. Since a complete thermocouple array was located only on one side wall of the test section, measurements for the staggered aperture configuration had to be done in two steps, reversing the inlet and outlet openings.

In each experimental run, the flow condition was set first and then heating was started. After that, the system was allowed to stabilize for about 15–20 min until the steady state was achieved. The flow, heat flux and thermocouple readings were then recorded. The ambient thermocouples were read at the beginning and end of each run to identify the transient effects or changes in the ambient temperature during the test. For each heat flux setting, the runs ranged from no

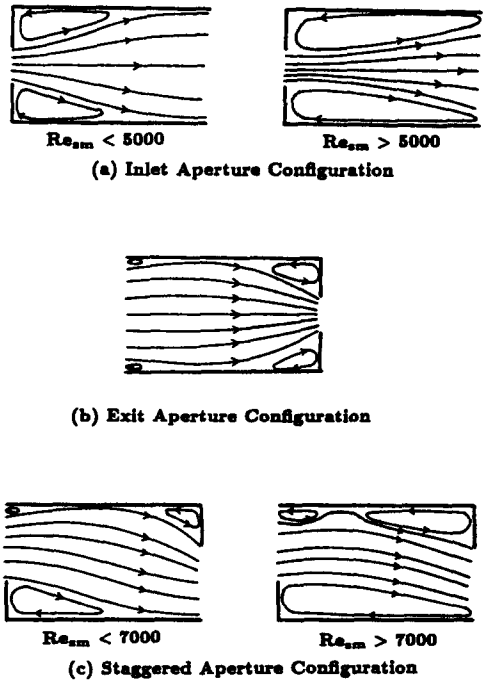

FIG. 3. Schematic of the core flow pattern for different aperture configurations.

flow (natural convection) to the highest flow that could be supplied by the pump.

The experimental measurements were analyzed using a data reduction computer program to calculate the local and average heat transfer coefficients. The data were checked for consistency in terms of the enhancement of heat transfer with flow rate and were discarded if any inconsistency was detected. Moreover, the uncertainty level for each experimental run was computed by the program. The uncertainty level for the Rayleigh number was always within 3%. The runs with a high uncertainty (more than 18%) on the local or average heat transfer coefficient were discarded. However, most accepted runs had a much smaller uncertainty (within 5%) in the local heat transfer coefficient. The measurements were also checked for repeatability by randomly repeating certain runs. In all cases, the trend of the local heat transfer distribution and the value of the average heat transfer coefficient were found to be repeatable within their level of uncertainty.

In addition to the heat transfer measurements, flow visualization studies were performed using a gravity-driven dye injection system. Dye was stored above the test section in a bottle with a drip valve. A thin plastic tube connected the exit of the bottle to a brass injector tube with an inside diameter of approximately 1 mm. With the drip valve open, a stream of slowly moving dye was released into the flow at the location of the injector, which could be placed anywhere in the test section. The subsequent motion of the dye was then observed visually and documented using still photography. A water-soluble food color was used as the dye.

OBSERVED FLOW STRUCTURE

A series of flow visualization tests were done with different flow rates and both with and without any heat input along the side walls. Figure 3 shows schematic diagrams of the core flow structure for different inlet and exit configurations in the middle of the channel (vertically) away from the top and bottom walls. For the entire range of flow rates tested here, the entrance flow to the test section was smooth and laminar. The flow inside the enclosure was observed to be turbulent for $Re_{\bar{m}} > 2000$. Note that this Reynolds number is based on channel length rather than the hydraulic diameter. Since the flow in an enclosure has similarities with both pipe flow and flow along a flat plate, the Reynolds number based on diameter and that based on length both appear to have significance in describing the flow. The latter one will be chosen here since the heat transfer mechanism in this type of flow is generally confined to the boundary layer region near the heated side walls. However, for the tests described here, the two Reynolds numbers are related as

$$Re_d = 0.73 Re_{\bar{m}}. \quad (1)$$

Most heat transfer tests were done with flow rates that correspond to a value of $Re_{\bar{m}}$ larger than 850. This was required to preserve sufficient accuracy in the flow measurement with the available flow meter.

For the inlet aperture configuration, it was found that the flow expanded after entering the test section. At flow rates corresponding to $Re_{\bar{m}} < 5000$, the expanding flow impinged on the test section side walls resulting in a stagnation line at each wall. This line moved further downstream as the flow rate increased. At any particular flow rate, the location of the stagnation line was not completely steady; rather it fluctuated over a range of as much as 3 cm. Towards the inlet side of the stagnation line, the fluid adjacent to the wall moved in a direction opposite to the main flow at a much smaller velocity. This recirculating flow behind the expanding inlet flow has been observed in previous investigations of forced convection at an abrupt pipe expansion [18] or backward facing step [19]. The flow downstream of the stagnation line was unidirectional toward the exit. The horizontal velocity along the side wall appeared to be strongest near the exit end.

For $Re_{\bar{m}} > 5000$, the expanding fluid stream moved out of the test section into the exit plenum without causing any stagnation on the heated surface. This resulted in a backward recirculating flow all along the side wall as shown in Fig. 3(a). The velocity of the backward flow visually appeared to increase with the Reynolds number. At very high flow rates, additional small recirculation eddies were formed near the corner region adjacent to the entrance.

For the exit aperture configuration, the flow pattern generally had a structure like that shown in Fig. 3(b). It can be seen that a small recirculation zone is present right next to the entrance. This type of recirculation pattern was also observed by Johnson *et al.* [16] in a previous investigation with an open-ended enclosure. The inlet separation may be attributed to the contraction of flow as it enters from the storage tank to the test section. The inlet storage tank was about 3.5 times as wide as the test section. As the test fluid entered the test section from the tank, it first contracted slightly and then expanded to re-attach itself to the surface. The size of the separation region increased with the flow rate. In the experiments of Johnson *et al.* [16] it appeared that the separation zone attains a maximum length at $Re_{\bar{m}} = 6500$ and then decreases. In the present tests, no significant decrease in the separation length was found, perhaps because the flow pattern was more complex due to the presence of the aperture at the exit.

The flow, after re-attaching to the surface, moved toward the exit and separated again from the wall to accommodate the presence of the restriction at the exit. The turning of the flow appeared to happen at an earlier location when the flow rate was increased. A recirculation region which was larger than the one immediately adjacent to the entrance was observed at the corner. For the range of flow rates studied here, a

region of forward moving flow was always found to exist between the two separation regions. Compared to the inlet aperture configuration, the recirculation for the exit aperture configuration was generally much smaller in size.

The flow pattern in the staggered aperture configuration was found to be something of a combination of the above two flow situations. It is schematically sketched in Fig. 3(c). The main flow, after entering the test section, turned at an angle and tried to orient itself to the downstream conditions. In the inlet restriction side of the test section (which resembled a half inlet aperture configuration), a stagnation line was found to be present for $Re_{zm} < 7000$. For this condition, the side with the exit restriction had a tiny recirculation zone at the entrance and a relatively big separation zone at the corner. All the recirculation patterns increased in size with the flow rate. For $Re_{zm} > 7000$, the backward moving fluid stream encompassed the entire inlet restriction side and the stagnation line disappeared.

The flow patterns described above are characteristic of the horizontal flow over most of the central portion of the enclosure. As expected, these patterns break down near the top and bottom walls due to the presence of these surfaces. From the flow visualization studies, it was also apparent that the presence of heat transfer at the side walls does not strongly affect the horizontal flow pattern in the center of the enclosure. The patterns shown in Fig. 3 were observed irrespective of whether the side wall was heated or not. The heat transfer, however, superimposed a boundary layer-like flow very close to the vertical side walls. This flow appeared to be laminar even though the core flow in the enclosure was turbulent. The upward moving fluid stream turned away from the surface as it approached the ceiling. This turning motion appeared to occupy a larger region at a higher surface heat flux condition.

LOCAL HEAT TRANSFER COEFFICIENT

For each combination of flow rate and surface heat flux, the surface thermocouple readings and measured heat flux were used to determine the local heat transfer coefficient, h, at each of the 32 thermocouple locations. For each location, the ratio h/h_{nc} was also calculated, where h_{nc} is the local heat transfer coefficient for laminar natural convection flow adjacent to a semi-infinite flat vertical surface at the same vertical location and heat flux. The value of h_{nc} was calculated using the correlation of Fujii and Fujii [20]:

$$h_{nc} = \frac{k}{x}\left(\frac{Pr}{4+9Pr^{0.5}+10Pr}\right)^{1/5}(Ra_x^*)^{1/5}. \quad (2)$$

Hence the amount by which h/h_{nc} exceeds one indicates the enhancement of the local heat transfer coefficient due to forced convection effects.

The measured variation of h/h_{nc} over the instrumented vertical wall of the test section is plotted in Figs. 4–9 for different combinations of flow rate, heat flux and aperture orientation. These figures also indicate the relative location of the embedded thermocouples on the surface.

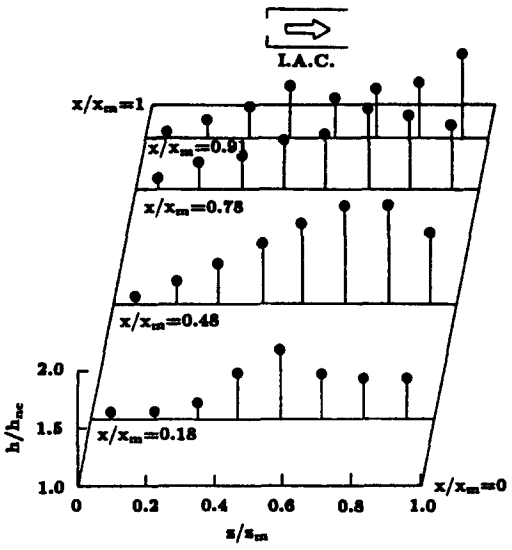

FIG. 4. Measured heat transfer enhancement for the inlet aperture configuration ($Ra_{zm}^* = 6.28 \times 10^{10}$, $Re_{zm} = 2250$).

Figure 4 shows the measured variation of h/h_{nc} for $Re_{zm} = 2250$ at a value of Ra_{zm}^* of 6.28×10^{10} for the inlet aperture configuration. At most vertical locations, the enhancement is found to increase with the horizontal distance up to a peak value at some intermediate location and then decrease slowly as the exist is approached. This distribution of heat transfer coefficient can be related to the observed flow pattern demonstrated in Fig. 3(a). Note that the Reynolds number here is below 5000, and consequently a stagnation line is present on the vertical side wall. The peak of the heat transfer coefficient corresponds to this stagnation line, where cold fluid from the center of the test section impinges on the side wall. To the entrance side of this stagnation line, the fluid close to the wall moves in a direction opposite to the main fluid stream, and a boundary layer-like flow structure is present with the stagnation line as the leading edge. The local heat transfer coefficient consequently decreases as the thickness of this boundary layer increases at locations further away from the stagnation line. The decrease of heat transfer enhancement on the exit side of the stagnation line is a consequence of a similar mechanism of the boundary layer development due to main stream flow.

It can also be seen that the horizontal variation of the heat transfer coefficient at the highest measurement location on the wall is somewhat different from the general trend seen at other locations. The behavior of the flow at this elevation is affected by the presence of the top wall of the enclosure. In Fig. 4 the maximum enhancement is seen to be about 1.8. Therefore, at

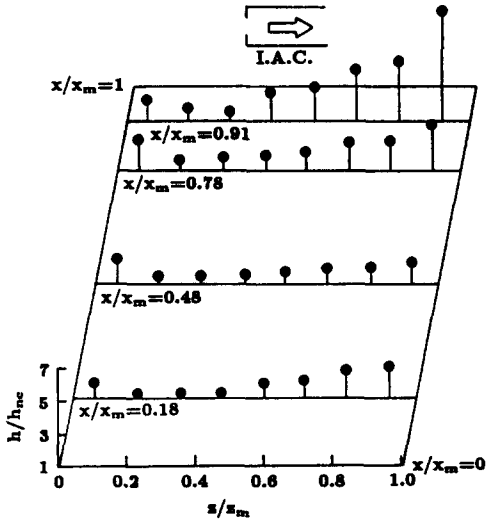

FIG. 5. Measured heat transfer enhancement for the inlet aperture configuration ($Ra^*_{xm} = 2.82 \times 10^{10}$, $Re_{zm} = 8200$).

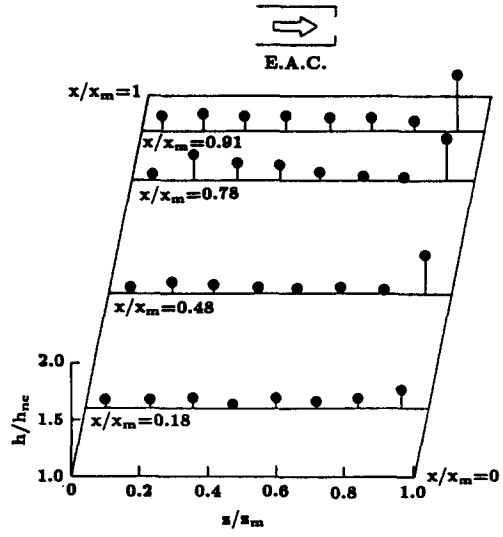

FIG. 6. Measured heat transfer enhancement for the exit aperture configuration ($Ra^*_{xm} = 3.38 \times 10^{10}$, $Re_{zm} = 880$).

$Re_{zm} = 2250$, the contribution of forced convection appears to be of a comparable order of magnitude to that of natural convection.

As mentioned before, the flow pattern changes at high Reynolds number (>5000) and the recirculation region then covers the entire heated wall. The distribution of the heat transfer coefficient is also altered. This can be seen in Fig. 5 where the local heat transfer enhancement values are plotted for $Re_{zm} = 8200$ for the inlet aperture configuration of the enclosure. The peak enhancement now occurs near the exit end of the heated wall. This happens because the recirculating back flow develops with the leading edge at the exit section, and the thickness of the boundary layer along the side wall increases as locations closer to the inlet of the test section are approached.

In Fig. 5 it can also be noticed that a second peak in the heat transfer enhancement occurs at the corner region next to the entrance doorway. This can be attributed to a small secondary circulation generated by the big recirculating flow covering the rest of the wall. This secondary flow was seen to occur only at large flow rates. Comparing Figs. 4 and 5, it can also be inferred that, as expected, the magnitude of the heat transfer enhancement is a strong function of Reynolds number. It was also found that the Rayleigh number has some influence on the enhancement. At the same Reynolds number, runs with low Rayleigh numbers were found to give a slightly higher enhancement than those with a high Rayleigh number. This can be explained on the basis of the interaction between the two convective mechanisms. Since the buoyancy-induced motion increases with Ra^*_{xm}, at a high heat flux, the flow in most regions of the wall becomes natural convection dominated and the forced flow has a relatively weaker effect than it does in weakly buoyant flows.

The distribution of the local heat transfer coefficient for the exit aperture configuration is shown in Figs. 6 and 7. Figure 6 corresponds to a low flow rate ($Re_{zm} = 880$). It can be seen that the enhancement in heat transfer beyond that for natural convection alone is small for this condition. In general, for all of the opening configurations tested here, for Re_{zm} values below 1500, the flow near the heated surface resembled pure natural convection laminar flow with a superimposed weak horizontal drift. This observation is consistent with previous experiments by Neiswanger *et al.* [17] for an enclosure with similar restrictions both at the inlet and the exit. The heat transfer increases with the horizontal flow rate. This is evident from Fig. 7 which corresponds to $Re_{zm} = 8900$ with about the same heat flux on the surface as that for Fig. 6. In both cases, it can be noticed that the

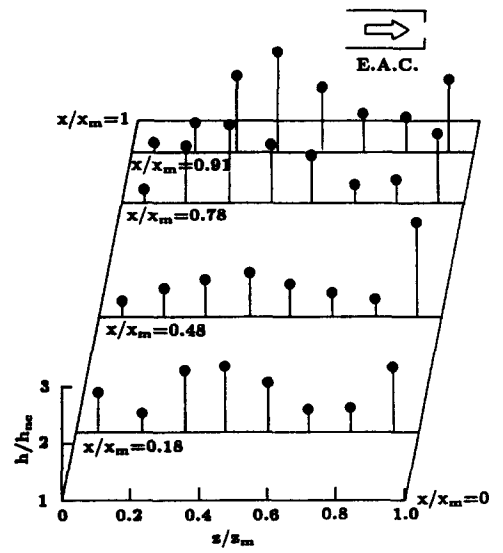

FIG. 7. Measured heat transfer enhancement for the exit aperture configuration ($Ra^*_{xm} = 3.68 \times 10^{10}$, $Re_{zm} = 8900$).

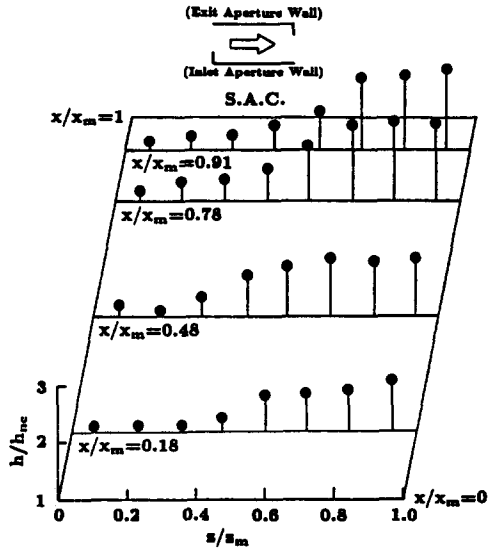

FIG. 8. Measured heat transfer enhancement on the inlet restriction wall for the staggered aperture configuration ($Ra^*_{zm} = 2.75 \times 10^{10}$, $Re_{zm} = 4000$).

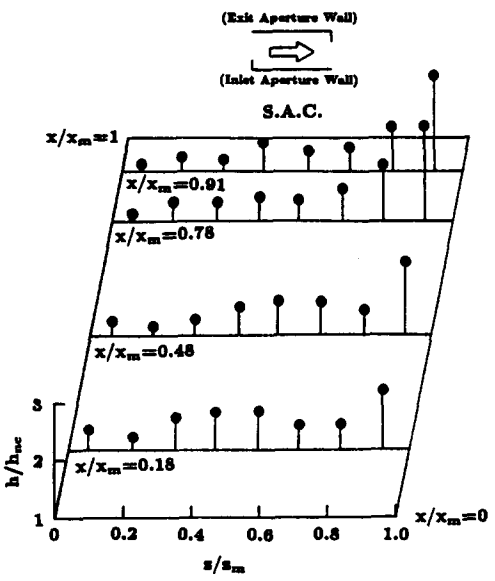

FIG. 9. Measured heat transfer enhancement on the exit restriction wall for the staggered aperture configuration ($Ra^*_{xm} = 3.12 \times 10^{10}$, $Re_{zm} = 4200$).

wall heat transfer coefficient has two peaks, one at the very end of the test section and another somewhere in the middle. The peak at the end is more prominent at a lower flow rate. This peak is associated with the recirculating flow at the corner region next to the exit section, as seen in flow visualization tests. When the main flow separates from the surface to accommodate the presence of the exit doorway, this recirculating eddy at the corner is produced, bringing in relatively cold fluid from the main stream into contact with the hot wall. The second peak is associated with the necking phenomenon as the fluid from the storage tank enters the test section, as shown in Fig. 3(b). The necking tends to increase the flow rate, and the main flow contacts the hot side wall at a progressively larger horizontal distance from the entrance as the flow rate increases. It can be seen that this peak enhancement occurs at a location further downstream in the case of $Re_{zm} = 8900$ than that for $Re_{zm} = 880$. Also, at a high flow rate, this first peak is of a comparable order of magnitude with the second peak seen near the exit end of the test section.

The local heat transfer enhancement for the case of a staggered aperture configuration for a particular set of Reynolds and Rayleigh numbers is plotted in Figs. 8 and 9 for the two heat transfer walls of the enclosure. The distribution of heat transfer coefficient in this case is somewhat similar to that observed for the symmetric doorway configurations. The inlet restriction wall, which resembles a portion of the inlet aperture configuration, has a distribution somewhat comparable to those observed in Figs. 4 and 5. Note that the Reynolds number here is 4000 and a stagnation line is present on this wall. As evident from the peak in heat transfer enhancement, this line is located very close to the exit section (at about $z/z_m = 0.8$) as opposed to the earlier location seen in Fig. 4. Upstream from this line, the heat transfer coefficient decreases due to the development of the boundary layer associated with the recirculating flow. However, in this case, the heat transfer coefficient downstream from this line is almost as high as that for the stagnation location. As discussed before, the location of the stagnation line fluctuated over a range of a few centimeters at high flow rates, resulting in a somewhat flatter peak in the measured data. Moreover, near the exit section, the fluid from the corner region moves toward the inlet restriction wall to pass through the exit aperture. This fluid stream pushes the boundary layer at the inlet restriction wall somewhat closer to the wall and reduces its thickness. This also enhances the heat transfer coefficient near the exit region. As seen in Fig. 9, the heat transfer at the exit restriction wall of the enclosure is somewhat similar in behavior to that for the exit aperture configuration. Note that in this case we also encounter two peaks, one near the end of the test section and the other at an intermediate location.

AVERAGE HEAT TRANSFER COEFFICIENT

The local heat transfer measurements were used to calculate the mean heat transfer coefficient over the entire heated surface. The surface was divided into 32 elements with a surface thermocouple at the center of each element. The mean heat transfer coefficient, $\bar{h}$, was then calculated as

$$\bar{h} = \frac{1}{x_m z_m} \sum_{i=1}^{32} A_i h_i \qquad (3)$$

where A_i is the area of the ith element and h_i the measured local heat transfer coefficient at the center

of the element. This summation approximates the integral average of h over the entire surface.

To develop a correlating equation to match $\bar{h}$ data calculated as described above, it was postulated here that the mixed convection heat transfer coefficient is given by

$$\bar{h} = (\bar{h}_{nc}^n + \bar{h}_{fc}^n)^{1/n} \quad (4)$$

where $\bar{h}_{nc}$ and $\bar{h}_{fc}$ are the mean heat transfer coefficients for the natural convection alone at the same heating condition and forced convection alone at the same flow condition respectively. This type of superposition approach has been successfully used to correlate heat transfer data for a wide variety of mixed convection flows [21, 22]. At low heat flux and high flow rates the flow is expected to be forced convection dominated so that $\bar{h} \approx \bar{h}_{fc}$. Conversely, at high heat flux and low flow rates, the flow is expected to be natural convection dominated and $\bar{h} \approx \bar{h}_{nc}$. Between these extremes, it is presumed that the overall h can be determined from a superposition of the two effects in the manner described by equation (4).

The average heat transfer coefficient due to natural convection alone was calculated from the measured values of the local heat transfer coefficient using equation (3). As mentioned before, the experimental measurements reported here included the natural convection limit in addition to mixed convection. Consequently, the values of $\bar{h}_{nc}$ reported here are actual measurements, in contrast to h_{nc}, which were computed using the heat transfer correlation of Fujii and Fujii [20]. In the limit of very high Reynolds number, the flow is expected to approach forced convection, with buoyancy effects being negligible. The highest Reynolds number used here was only about 9000. Therefore, the forced convection heat transfer coefficient could not be directly ascertained from the experimental data. The approach used here was a simultaneous optimization of the assumed form of mixed convection and forced convection correlations. The mixed convection correlation used here has already been mentioned in equation (4). The forced convection was assumed to be of the form

$$\bar{h}_{fc} = a\left[\frac{k}{z_m}\right] Pr^{0.6}\, Re_{z_m}^b. \quad (5)$$

The assumption of this correlation form is based on the commonly used correlation for turbulent forced convection boundary layer flow at moderate Prandtl numbers, proposed by Kays and Crawford [23]. Here the Prandtl number is assumed to have an exponent of 0.6. Since the core flow at a high Reynolds number appeared to be turbulent and the flow near the wall is boundary layer in structure, this flow may have a similar Prandtl number dependence as the turbulent boundary layer flow. This point, however, was not verified by our data since they do not span a wide range of Prandtl numbers. All the data reported here correspond to values of Pr between 5.9 and 7.4.

Table 1. Constants for heat transfer correlations for different aperture configurations (equations (4) and (5))

Enclosure geometry	n	a	b
Inlet aperture configuration	3.7	0.071	0.78
Exit aperture configuration	1.8	0.0006	1.26
Staggered aperture configuration	3.0	0.072	0.79

It can be seen that equations (4) and (5) contain four unknowns, namely n, $\bar{h}_{fc}$, a and b. The optimization approach used here was a simultaneous linear regression fit on $\bar{h}_{fc}$ and minimization of least square error on predicted values of $\bar{h}$. The overall regression scheme was as follows. First, a value of n was guessed. Then, equation (4) was used to calculate a set of $\bar{h}_{fc}$ from measured values of $\bar{h}$ and $\bar{h}_{nc}$. Next, these $\bar{h}_{fc}$ and measured values of Re_{z_m} were used to determine a and b values which minimized the error in $\bar{h}_{fc}$ in the least square sense. Equations (4) and (5) were used to compute corresponding predicted values of $\bar{h}$. The errors in the prediction of $\bar{h}$ were then calculated for each data point. The value of n which resulted in the minimum total squared error for all the data points was chosen for the correlation. The values of n, a and b for the different enclosure configurations tested here are listed in Table 1.

The experimentally determined $\bar{h}$ values for the heated side walls of the enclosure are compared with the corresponding proposed correlations in Figs. 10–12 for the three different opening configurations. It can be seen that the overall agreement between the measured data and the correlations is quite good. However, at low values of $\bar{h}_{fc}/\bar{h}_{nc}$, when the flow velocity is small, the data are seen to deviate somewhat from the correlations. The correlations underestimate heat transfer in such situations. Also, the difference between the prediction and experimental data is somewhat larger in magnitude for the inlet aperture con-

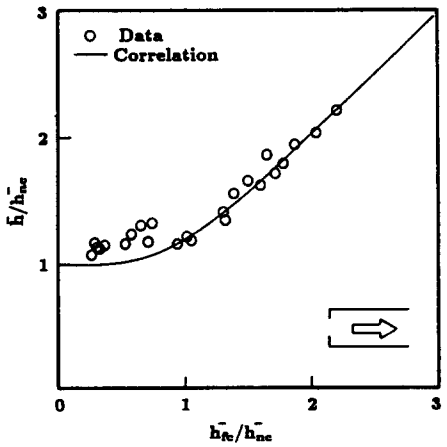

FIG. 10. Comparison of experimental mean heat transfer coefficients with the proposed correlation for the inlet aperture configuration.

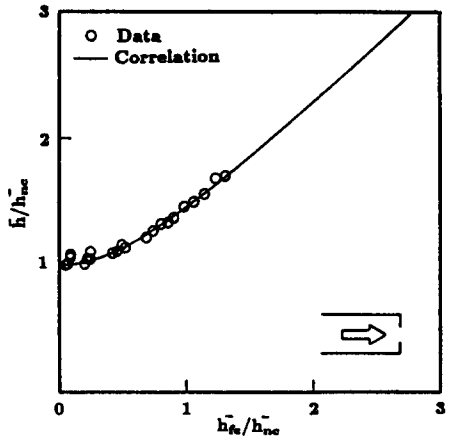

FIG. 11. Comparison of experimental mean heat transfer coefficients with the proposed correlation for the exit aperture configuration.

figuration. It may be recalled here that when a restriction is present at the entrance section of the enclosure, the side wall next to that restriction usually has a stagnation line where cold fluid from the core impinges on the hot wall. This stagnation is present at low flow rates and disappears when the flow velocity is sufficiently increased.

In the case of the inlet aperture configuration, the inlet restriction is present next to both side walls and therefore this geometry has the highest stagnation effect at low flow rates. Note also that the simple correlation proposed here expresses mixed convection heat transfer as a function of forced and natural convection heat transfer coefficients. In both these limiting cases, no phenomenon such as impingement of fluid on the surface is present. Consequently, the correlation cannot directly account for the stagnation line phenomena in the flows. Since the physics of the flow impingement and the resulting enhancement of heat transfer are not well understood at the present time, we have elected to use the simple correlation form proposed here, keeping in mind its limitations. Moreover, the difference in magnitude between the present data and the correlation are small and fall within the uncertainty limit of the experiment.

It can be seen in Figs. 10–12 that, as expected, the data approach the natural convection limit ($\bar{h}/\bar{h}_{nc} = 1$) at small values of Γ, and the forced convection limit ($\bar{h}/\bar{h}_{nc} = \Gamma$) at large values of Γ. It is possible, therefore, to distinguish between the natural, mixed and forced convection regimes by comparing the correlation predictions of $\bar{h}/\bar{h}_{nc}$ with these limits. The natural convection regime was arbitrarily taken to correspond to conditions for which $\bar{h}$ is within 5% of its value for natural convection alone at the specified heat flux. Since this implies that $1.0 < \bar{h}/\bar{h}_{nc} < 1.05$, the value of Γ which corresponds to the natural to mixed convection boundary can be calculated using equation (4). In a similar way, the forced convection regime was taken to correspond to conditions where $\bar{h}$ is within 5% of its value for purely forced convection flow at the same flow rate. This boundary between mixed and forced convection regimes can be solved by simultaneously solving equation (4) and the relation $\bar{h}/\bar{h}_{nc} = 1.05\Gamma$. Mixed convection exists between these two transition boundaries. The flow regime map along with the transition lines are graphically represented in Figs. 13–15 for the different aperture configurations tested here. The data points indicate all the combinations of Re_{zm} and Ra^*_{xm} for which experiments were done in the present study. It may be noticed that at the same flow rate and heat flux conditions, the flow regime encountered may be different for different opening configurations. This indicates that the flow inside a partial enclosure may be quite sensitive to inlet and exit geometry, and the design of doorways may have a crucial impact on the heat transfer from the walls in a building.

CONCLUSIONS

Orthogonal mixed convection flow in a partial enclosure with different inlet and exit aperture con-

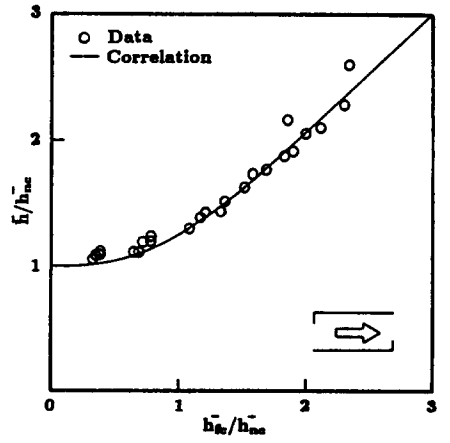

FIG. 12. Comparison of experimental mean heat transfer coefficients with the proposed correlation for the staggered aperture configuration.

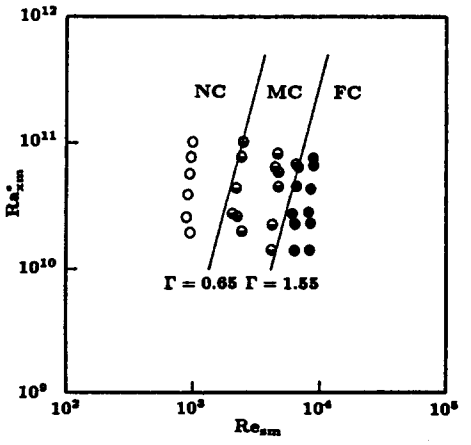

FIG. 13. Flow regime map for the inlet aperture configuration.

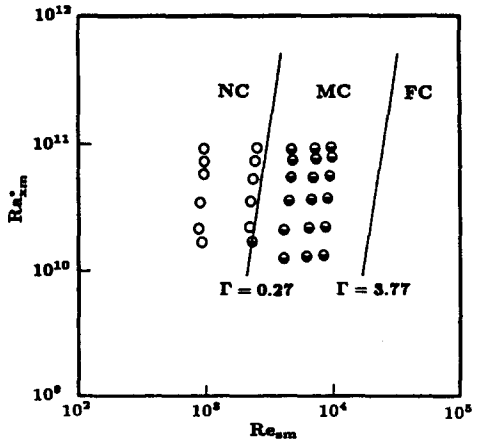

FIG. 14. Flow regime map for the exit aperture configuration.

figurations has been investigated. Experiments were conducted at high Rayleigh numbers and low to moderate Reynolds numbers with uniformly heated side walls and adiabatic top and bottom walls. The flow inside the enclosure was found to depend on the aperture configuration and the flow rate of the incoming fluid. The local heat transfer from the vertical side wall was found to be intimately related to the flow structure next to the wall, where a buoyancy driven upward motion interacted with the direct or recirculating horizontal flow.

For the inlet aperture configuration, at $Re_{zm} < 5000$, the flow impinges on the vertical side walls forming a stagnation line on each wall. The heat transfer coefficient is highest at this stagnation location. Upstream from this stagnation line, the flow close to the vertical wall moves in a direction opposite to the main flow developing a boundary layer-like flow structure. Downstream from this stagnation line, another boundary layer-like flow develops due to the main stream fluid flow. The heat transfer coefficient

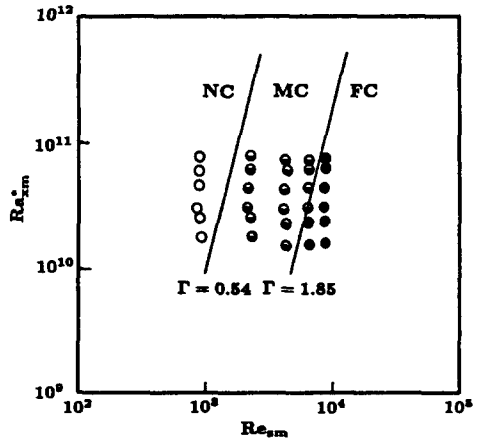

FIG. 15. Flow regime map for the staggered aperture configuration.

at this condition decreases in both directions from the stagnation line. At $Re_{zm} > 5000$, the incoming fluid velocity is so high that the expanding flow goes out of the test section before impinging on the hot side walls. A recirculating back flow encompasses the entire wall in such a situation. The heat transfer enhancement is found to be highest at the exit region and gradually decreases toward the entrance. At a very high flow rate, a small secondary flow is found at the corner region next to the entrance. This also enhances the heat transfer coefficient to some extent at the corner.

In the case of the exit aperture configuration, the recirculating flow is found to be absent in the intermediate region of the enclosure. A recirculating cell appears at the corner region prior to the exit opening. This is formed due to the turning of the main flow away from the wall to accommodate the presence of the aperture. In this region, the heat transfer is found to be high due to entrainment of the cold fluid by the recirculating flow and impingement of it on the surface. The heat transfer at the entrance region of the enclosure is dictated by necking of the flow as it enters from the storage tank to the test section. The reattachment of the flow after necking also results in a relatively larger heat transfer coefficient.

In the case of a staggered aperture configuration, the flow pattern and the corresponding distribution of the local heat transfer coefficient were found to be something of a combination of those for the inlet and exit aperture geometries. The staggered orientation of the openings causes the main flow to move at an angle while passing through the test section. A stagnation line was found to be present on one of the side walls (inlet aperture wall) when the flow rate corresponded to $Re_{zm} < 7000$.

The measured local heat transfer coefficients were also used to calculate the mean heat transfer coefficient for each combination of heat flux and flow conditions. A simple correlating equation was developed for each enclosure geometry, which agreed favorably with the measurements. The limitations of these correlations were explored. A map for predicting the flow regime was developed for each enclosure aperture configuration. In these maps, the flow was identified as mixed convection when the average heat transfer coefficient deviated by more than 5% from natural convection with the same heat flux and from forced convection with the same flow rate. The results of this study provide new insight into the manner in which geometry variations affect flow behavior and heat transfer mechanisms for orthogonal mixed convection. However, because the transport exhibits a strong geometry dependence, the conclusions derived here regarding the flow and heat transfer coefficient may be applicable only to similar geometries and flow conditions.

Acknowledgement—Support for this work was provided by National Science Foundation under grant number CBT-8451781.

REFERENCES

1. S. T. McComas and E. R. G. Eckert, Combined free and forced convection in a horizontal circular tube, *ASME J. Heat Transfer* **88**, 147–153 (1966).
2. Y. Mori, K. Futagami, S. Tokunda and M. Nakamura, Forced convective heat transfer in uniformly heated horizontal tubes: 1st Report—experimental study on the effects of buoyancy, *Int. J. Heat Mass Transfer* **9**, 453–463 (1966).
3. B. S. Petukov and A. F. Polyakov, Experimental investigation of viscogravitational fluid flow in a horizontal tube, *High Temperature* **5**, 75–81 (1967).
4. R. L. Shanon and C. A. Depew, Combined free and forced laminar convection in a horizontal tube with uniform heat flux, *ASME J. Heat Transfer* **90**, 353–357 (1968).
5. A. E. Bergles and R. R. Simonds, Combined forced and free convection for laminar flow in horizontal tubes with uniform heat flux, *Int. J. Heat Mass Transfer* **14**, 1989–2000 (1971).
6. S. W. Hong, S. M. Morcos and A. E. Bergles, Analytical and experimental results for combined forced and free laminar convection in horizontal tubes, *Proc. 5th Int. Heat Transfer Conf.*, Vol. 3, pp. 154–158 (1974).
7. S. M. Morcos and A. E. Bergles, Experimental investigation of combined forced and free convection in horizontal tubes, *ASME J. Heat Transfer* **97**, 212–219 (1975).
8. W. M. Yousef and J. D. Tarasuk, Free convection effects on laminar forced convection heat transfer in a horizontal isothermal tube, *ASME J. Heat Transfer* **104**, 145–152 (1982).
9. J. W. Ou and K. C. Cheng, Natural convection effects on Graetz problem in horizontal isothermal tube, *Int. J. Heat Mass Transfer* **20**, 953–960 (1977).
10. K. C. Cheng and J. W. Ou, Free convection effects on Graetz problem for large Prandtl number fluids in horizontal tubes with uniform heat flux, *Proc. 5th Int. Heat Transfer Conf.*, Vol. 3, pp. 159–163 (1974).
11. M. Hishida, Y. Nayano and M. S. Montesclaros, Combined forced and free convection in the entry region of an isothermally heated horizontal pipe, *ASME J. Heat Transfer* **104**, 153–159 (1982).
12. L. S. Yao, Forced-free convection in the entry region of a heated straight pipe, *ASME J. Heat Transfer* **100**, 212–219 (1976).
13. J. W. Ou, K. C. Cheng and R. C. Lin, Natural convection effects on Graetz problem in horizontal rectangular channels with uniform wall temperature for large *Pr*, *Int. J. Heat Mass Transfer* **17**, 835–843 (1974).
14. K. C. Cheng, S. W. Hong and G. J. Hwang, Buoyancy effects on laminar heat transfer in the thermal entrance region of horizontal rectangular channels with uniform wall heat flux for large Prandtl number fluids, *Int. J. Heat Mass Transfer* **15**, 1819–1836 (1972).
15. M. M. M. Abou-Ellail and S. M. Morcos, Buoyancy effects in the entrance region of horizontal rectangular channels, *ASME J. Heat Transfer* **105**, 924–928 (1983).
16. G. A. Johnson, L. Neiswanger and V. P. Carey, Cross-flow mixed convection at high Rayleigh number in an open-ended rectangular enclosure, ASME Paper No. 86-WA/HT-99 (1986).
17. L. Neiswanger, G. A. Johnson and V. P. Carey, An experimental study of high Rayleigh number mixed convection in a rectangular enclosure with restricted inlet and outlet openings, *ASME J. Heat Transfer* **109**, 446–453 (1987).
18. R. S. Amano, M. K. Jensen and P. Goel, A numerical and experimental investigation of turbulent heat transport downstream from an abrupt pipe expansion, *ASME J. Heat Transfer* **105**, 862–869 (1983).
19. J. C. Vogel and J. K. Eaton, Combined heat transfer and fluid dynamic measurements downstream of a backward-facing step, *ASME J. Heat Transfer* **107**, 922–929 (1985).
20. T. Fujii and M. Fujii, The dependence of local Nusselt number on Prandtl number in the case of free convection along a vertical surface with uniform heat flux, *Int. J. Heat Mass Transfer* **19**, 121–122 (1976).
21. S. W. Churchill and R. Usagi, A general expression for the correlation of rates of transfer and other phenomena, *A.I.Ch.E. Jl* **18**, 1121–1128 (1972).
22. D. L. Siebers, R. G. Schwind and R. J. Moffat, Experimental mixed convection heat transfer from a large vertical surface in a horizontal flow, Sandia National Laboratories, SAND 83-8225, Livermore, California (1983).
23. W. M. Kays and M. E. Crawford, *Convective Heat and Mass Transfer*. McGraw-Hill, New York (1980).

ETUDE EXPERIMENTALE DE LA CONVECTION MIXTE ORTHOGONALE DANS UNE CAVITE PARTIELLE

Résumé—On présente des mesures des coefficients locaux de transfert thermique et des résultats de visualisation d'écoulement pour la convection mixte orthogonale dans une cavité partielle ayant des parois latérales uniformément chauffées et les parois supérieure et inférieure adiabatiques. Dans cette étude on utilise de l'eau comme fluide dans une petite cellule avec différentes configurations d'entrée et de sortie. Les conditions sont choisies pour simuler un nombre de Rayleigh élevé (10^{10}–10^{11}) et un nombre de Reynolds faible ou modéré (0–9000) comme dans les applications de la thermique du bâtiment. Quand le débit à travers la cavité augmente, l'excès de transfert thermique par rapport à la convection naturelle seule augmente aussi. L'accroissement local est parfois, dans certaines situations, multiplié par 7. La variation du coefficient local de transfert sur la surface chauffée est fortement affectée par des zones de recirculation de l'écoulement forcé dans la cavité et aussi par des écoulements d'impact ou de séparation dans certaines régions des parois latérales. Des coefficients de transfert moyens sont donnés pour les parois latérales. Le plus fort accroissement moyen est de 2,6 pour $Ra = 1{,}6 \times 10^{10}$ et $Re = 8740$ avec une orientation décalée des ouvertures d'entrée et de sortie. On propose aussi des formules pour le coefficient moyen de transfert et une carte de régime d'écoulement pour différentes géométries.

EXPERIMENTELLE UNTERSUCHUNG DER ORTHOGONALEN MISCHKONVEKTION IN EINEM TEILWEISE GESCHLOSSENEN HOHLRAUM

Zusammenfassung—Es werden die Ergebnisse von Wärmeübergangsmessungen und einer Sichtbarmachung der Strömung für orthogonale Mischkonvektion in einem teilweise geschlossenen Hohlraum vorgestellt. Die Seitenwände sind dabei gleichförmig beheizt, die obere und untere Abdeckung adiabat. Als Versuchsstoff wird Wasser verwendet, die Versuchskammer ist verhältnismäßig klein und wird mit unterschiedlichen Einlaß- und Auslaßbedingungen betrieben. Die Strömungs- und Beheizungsbedingungen werden so gewählt, daß hohe Rayleigh-Zahlen (10^{10}–10^{11}) und kleine bis mittlere Reynolds-Zahlen (0–9000) erreicht werden. Diese Bereiche sind typisch für den Wärmeübergang in Gebäuden. Bei zunehmender Strömungsgeschwindigkeit nimmt auch die Verbesserung des Wärmeübergangs über denjenigen bei reiner natürlicher Konvektion zu. In manchen Strömungssituationen erreicht die örtliche Erhöhung den Faktor 7. Es zeigt sich, daß die Veränderung der örtlichen Wärmeübergangskoeffizienten an der Heizfläche stark von Rückströmungen in der erzwungenen Hauptströmung in dem Hohlraum beeinflußt wird. Starke Auswirkungen hat auch das Auftreffen der Strömung auf die Seitenwände oder die Ablösung der Strömung an diesen Wänden. Es werden mittlere Wärmeübergangskoeffizienten für die Seitenwände vorgestellt, die durch eine Mittelwertbildung aus gemessenen örtlichen Werten über die Heizfläche bestimmt wurden. Der größte Erhöhungsfaktor für die Mittelwerte beträgt 2,6, bei $Ra = 1{,}6 \times 10^{10}$ und $Re = 8740$ für nichtfluchtende Anordnung von Einlaß- und Auslaßöffnung. Schließlich wird eine Korrelation für den mittleren Wärmeübergangskoeffizienten vorgeschlagen und eine Karte der Strömungsformen für unterschiedliche Hohlraumgeometrien.

ЭКСПЕРИМЕНТАЛЬНЫЕ ИЗМЕРЕНИЯ ОРТОГОНАЛЬНОЙ СМЕШАННОЙ КОНВЕКЦИИ В ЧАСТИЧНО ЗАМКНУТОЙ ПОЛОСТИ

Аннотация—Описываются измерения локальных коэффициентов теплопереноса и результаты экспериментов по визуализации течения при ортогональной смешанной конвекции в частично замкнутой полости с рднородно нагреваемыми боковыми и адиабатическими верхней и нижней стенками. Опыты проводились в экспериментальном модуле малого масштаба с различными конфигурациями вдува и стока и использованием воды в качестве рабочей жидкости. Условия течения и нагрева выбирались для моделирования высоких значений числа Рэлея (10^{10}–10^{11}), а также низких и умеренных значениях числа Рейнольдса (0–9000), характерных для приложений в строительной теплофизике. С ростом скорости прокачки через полость интенсификация теплоотдачи по сравнению со случаем чисто свободной конвекции также нарастает. Для некоторых условий течения локальный теплоперенос усиливается до 7 раз. Найдено, что на изменение локального коэффициента теплоотдачи над нагретой поверхностью сильное влияние оказывают рециркуляция в некоторых областях вынужденного течения внутри полости, а также натекание потока на боковую стенку или отрыв от нее в некоторых областях. Представлены также средние коэффициенты теплоотдачи для боковых стенок, определенные методом усреднения измеренных локальных значений теплоотдачи над нагретой поверхностью. В среднем максимальная интенсификация процесса достигает 2,6 при $Ra = 1{,}6 \times 10^{10}$ и $Re = 8740$ в случае шахматного расположения отверстий входа и выхода. Предложены соотношения для среднего коэффициента теплоотдачи, а также картина течения при различных геометриях полости.